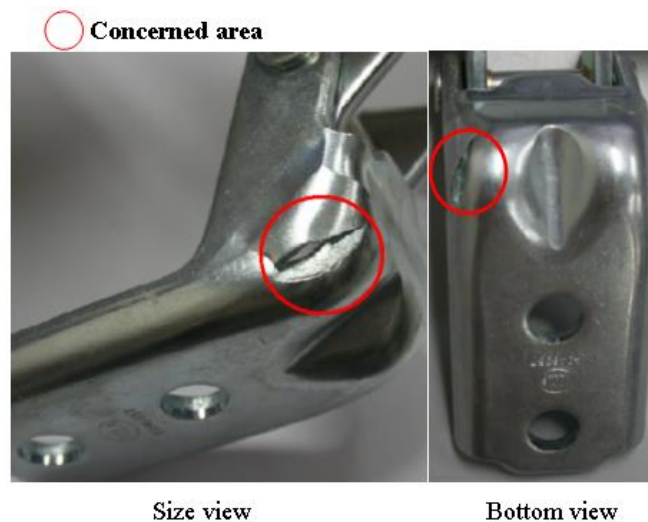


## *Chapter 3: Application of Proposed Hardening Model to Predict Fracture and Improve Press Formability of Door Hinge*

### **3.1 Introduction**

Door hinges are a key product in the automotive industry, and their functions include not only opening and closing the door or keeping the door open at a certain angle, but also reducing passenger trauma in the case of a collision. Car door hinges are produced by punching and then forming a plate to obtain the desired geometry. Door hinges can take many shapes, depending on the type of automobile, front or rear door, designer, and producer. In addition, there are many processing parameters that contribute to the formability of a door hinge, such as the material properties, forming conditions, geometric shapes of the die and punch, and geometric shapes of the blanks etc., which in turn determine the press formability, as regards the thickness variation, and blank failure after the forming. However, due to the increasing demand for light-weight, high-strength and corrosion-resistant materials, many new materials have been developed for application in automobiles. Yet, these materials, especially high-strength steel sheet, tend to have less formability than the conventional materials used for sheet forming, resulting in the frequent failure of door hinge products. When manufacturing a door hinge, as shown in Figure 3.1, product failure frequently occurs in the critical area when subjected to serious strain during the forming process and found to be prone to internal or superficial micro-defects due to excessive tensile stress [36]. This initial damage and its growth then cause quality problems, such as necking and fractures, due to ductile tearing of the sheet.



**Figure 3.1:** Typical failure of a door hinge in critical area

To predict material fractures several researches had been proposed [37, 38]. Among the various methods, Clift et al. [39] concluded that the existing ductile fracture criteria were more accurate than other methods. To improve the formability of sheet material, Kim and Park [40] used FE simulations according to the orthogonal array of Taguchi's method [41-43] to determine the effect of forming variables on the stamping formability and investigate the effect of design variables on the quality characteristics of the product. Nguyen *et al.* [44] improved the press formability of a door hinge by changing the shape of the concerned area of the blank based on FE simulations. Furthermore, to improve the efficiency of sheet metal forming optimization, the meta-modeling technique is introduced. The meta-modeling technique is a method for replacing a complex model by an approximate one based on results calculated at various samples in the design space. Several meta-modeling techniques will be effective for the engineering optimization. These methods have been reviewed by Wang and Shan [45] in detail. See other literatures [46] and applications [48, 49] for further meta-modeling techniques. Accordingly, this application improves the door hinge press formability by changing the geometric shape of the die and bead punch in the concerned area. Fracture prediction using the finite element method is an easy and efficient way to apply ductile fracture criteria and determine the influence of changing the geometric parameters of the die and bead punch. In the near future studies, meta-modeling techniques will be applied to solve optimization problems in a certain design space and having certain constraints.

In this application, the forming process of a door hinge is simulated using ABAQUS/Explicit finite element code [32]. As the ductile failure criterion, the Oyane fracture criterion [50] via VUMAT user material based on a combined isotropic and kinematic hardening law is applied to improve the press formability of the door hinge. It is show to be a realistic and cost effective method. The FE simulation result for a cracked test sample are presented in Figure 3.2, where integral value I was calculated from the definition of the accumulated damage according to the Oyane ductile criterion.

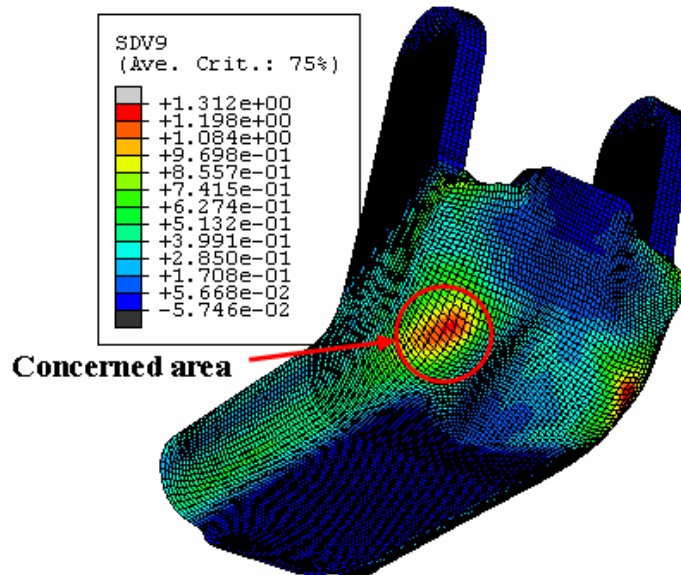


**Figure 3.2:** Deformed shape in finite element simulation, where maximum of integral value I was 1.343 in concerned area

The effect of the die and bead punch geometries are then investigated to determine their influence on the press formability and the results demonstrate the ability to predict when and where ductile damage will appear in the workpiece during the forming operation. Finally, the improved geometry is presented according to Taguchi's experimental technique to achieve the improved shape for the concerned area in the die and bead punch.

## 3.2 Finite element procedures

### 3.2.1 Materials

Table 3.1 shows the mechanical properties of the blank, SAPH-440 sheet steel with a thickness of 5mm. The parameters characterizing the uniaxial-stress-plastic-strain response of the material used in the FE simulations are also given in the Table in terms of the parameters in Swift's work-hardening law [51], using the following expression:

$$\bar{\sigma} = K(\varepsilon_0 + \bar{\varepsilon}_p)^n \quad (3.1)$$

Where K is the plastic coefficient, n is the work-hardening exponent, and  $\bar{\sigma}$ ,  $\bar{\varepsilon}_p$ ,  $\varepsilon_0$  are the equivalent stress, equivalent strain, and yield strain, respectively.

**Table 3.1:** Mechanical properties of tested material (SAPH-440)

Material	SAPH-440
Density ( $\rho$ , kg/mm <sup>3</sup> )	7.8e-09
Young's modulus (E, kN/mm <sup>2</sup> )	210
Tensile strength (MPa)	380
$\varepsilon_0$	0.0078
K (MPa)	832.85
n-value	0.182

### 3.2.2 Ductile fracture criterion

Based on various hypotheses, certain criteria have already been proposed for ductile fractures [39, 52]. Oyane et al. [50] proposed a criterion allowing for the history of the hydrostatic stress affecting the occurrence of a ductile fracture, and this has been widely applied in the field of bulk forming with a high reliability [50, 52]. This criterion has also been used by Takuda et al. [53] to predict fracture initiation for the deep drawing processes of laminated composite sheets. The results were successful for the fracture prediction. Yet, it should be mentioned that the application of the ductile fracture criterion is more effective for low ductility materials. Thus, in the present study, the criterion of Oyane et al. [50] is employed in Equation (3.2):

$$\int_0^{\bar{\varepsilon}_f} \left( \frac{\sigma_m}{\bar{\sigma}} + C_1 \right) d\bar{\varepsilon} = C_2 \quad (3.2)$$

where  $\bar{\varepsilon}_f$  is the equivalent strain at which the fracture occurs,  $\sigma_m$  is the hydrostatic stress,  $\bar{\sigma}$  is the equivalent stress,  $\bar{\varepsilon}$  is the equivalent strain, and  $C_1$ ,  $C_2$  are the material constants.

To determine the material constants  $C_1$ ,  $C_2$  in Equation (2), destructive tests have to be operated under at least two types of stress conditions. Thus, the present study refers to the testing results of Ko et al. [54], where  $C_1$ ,  $C_2$  are simply determined by uniaxial and plane-strain tension tests [53]. The fracture strain for uniaxial tension and a plane strain state using a dome test was 0.7156 and 0.5686, respectively. From this result, the material constants  $C_1$ , and  $C_2$  for the ductile fracture criterion were calculated as 1.9438, and 2.3831, respectively.

### 3.2.3 Combination of finite element simulation and criteria for ductile fracture

Figure 3.3 shows the finite-element model of ABAQUS version 6.5 for the forming test process. Here, the punch and die model were made from the shape of the product using CATIA software, the blank modeled using solid elements C3D8R, and the punch and die modeled using rigid surface-elements R3D4 with three integration points. Throughout this study, a uniform mesh was used for both the solid and rigid surface-elements. The average element size of the solid elements was about 1mm in width, 1mm in length, and 1mm in height. Meanwhile, the average element size of the rigid surface-elements was about 1 mm in width, and 1 mm in length.

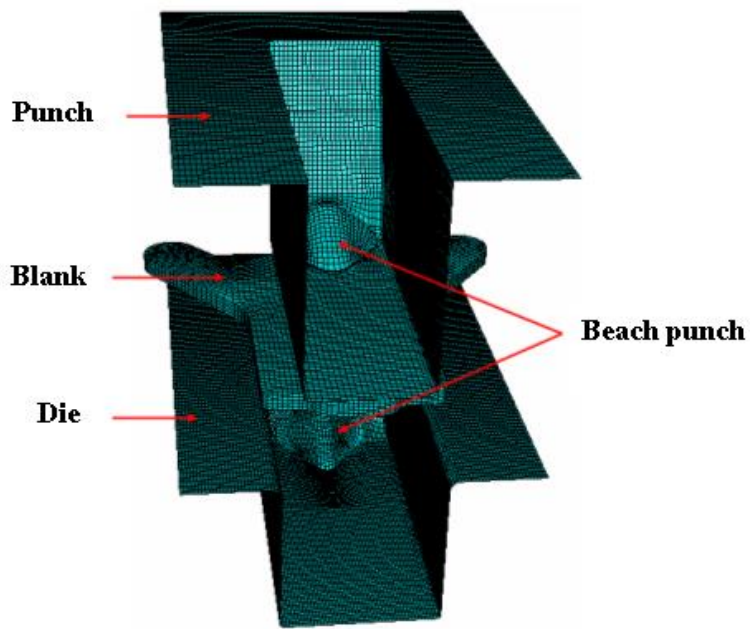


**Figure 3.3:** Finite element model for test simulation

The friction behavior of the blank-die/blank-punch was modeled using the Coulomb friction law. The friction coefficient  $\mu_1$  of the blank at the blank-die interface was measured using an automatic draw bead simulation [40], which was developed to simulate the friction state of a specimen under a drawing deformation mode. The test results revealed that the friction coefficient at the blank-die interface were within the range of  $\mu_1=0.1$  to 0.2. However, for the friction coefficient  $\mu_2$  at the blank/punch interface,  $\mu_2=0.25$ , was assumed for all the simulations as in Reference [44].

In the simulation, for an elastic/plastic material with a combination of isotropic and kinematic hardening that obeys the von Mises yield criterion, the Equations (2.48-2.59) are valid if the strain rate and stress rate remain constant during a finite yet very small time increment  $\Delta t$ .

The value for  $\Delta\gamma$  of Equation (2.57) is used in the incremental Equation to determine  $\sigma_{new}$ ,  $\sigma_{new}^m$ , and  $\bar{\epsilon}^{pl}$ . These formulations are combined with the criterion of Oyane in Equation (3.2) and coded into a VUMAT subroutine, for use in ABAQUS/Explicit. When rewriting the criteria for a ductile fracture in Equation (3.2), the following integral is obtained:

$$I = \frac{1}{C_2} \int_0^{\bar{\epsilon}^f} \left( \frac{\sigma_m}{\bar{\sigma}} + C_1 \right) d\bar{\epsilon} \quad (3.3)$$

The histories of stress and strain in each element during forming are calculated using the FEM, and the ductile fracture integral  $I$  in Equation (3.3) is obtained for each element. When the integral value  $I$  of Equation (3.3) reaches 1.0, a fracture will occur. This ductile fracture value  $I$  can be calculated for every finite element during the forming process. Figure 3.4 shows the general updating flow-chart of the VUMAT subroutine implemented in ABAQUS.

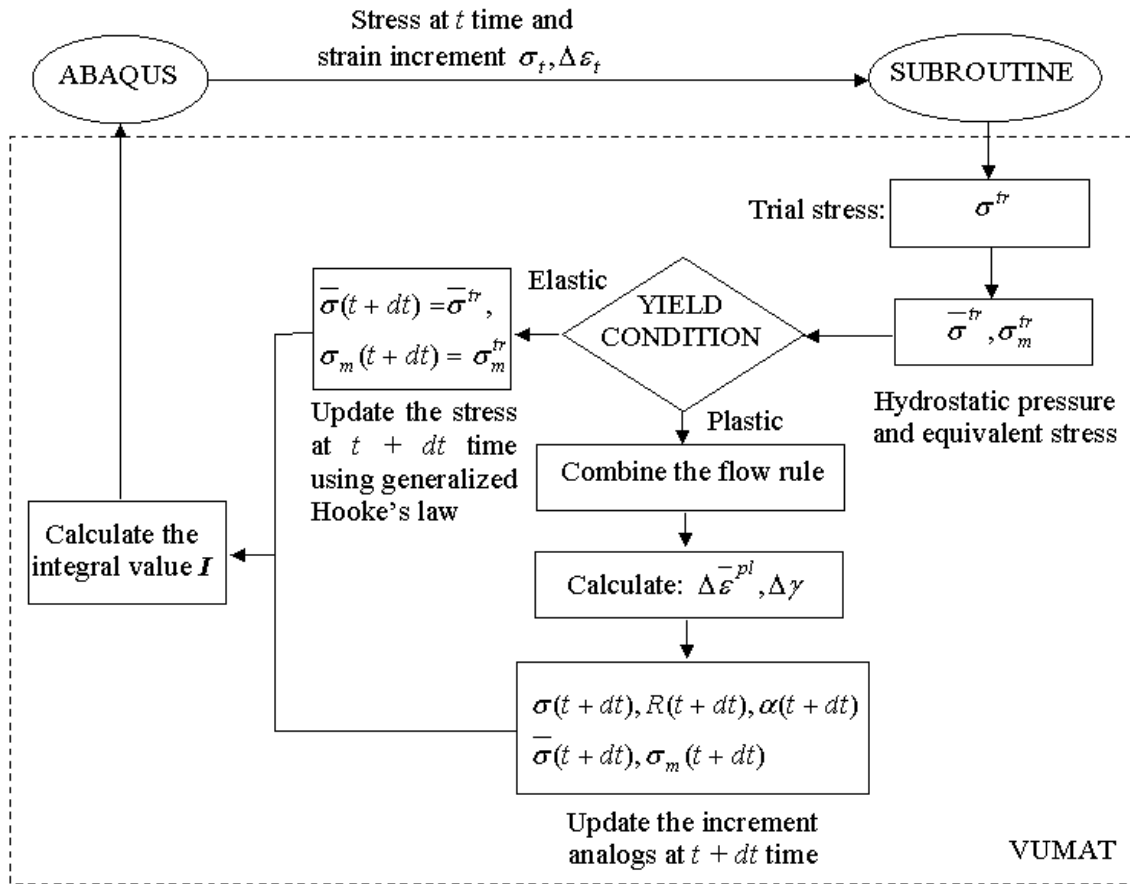


Figure 3.4: The general updating flow-chart of subroutine

### 3.3 Taguchi's Orthogonal Array

When manufacturing a door hinge manufacturing, fractures tend to occur near the punch corner of the blank. The reason for this is that the high tensile stress and equivalent plastic strain at the punch corner are larger than those in the other zones of the blank. When changing the geometry of the die and bead punch in the concerned area, it was found that the magnitude of the von-Mises stress and equivalent plastic strain were also changed. Therefore, the integral value  $I$  was changed. Thus, it was concluded that the geometry of the die and bead punch for the concerned area in the blank could be improved.

When using this characteristic, the problem becomes a smaller-the-better type problem according to the Taguchi method, which means the smaller the integral value  $I$ , the better the press formability.

The signal-to-noise ratio ( $S/N$  ratio) defined according to the Taguchi method is:

$$\eta_i(\text{dB}) = -10 \log_{10}(I^2) \quad (3.4)$$

where  $\eta$  denotes the observed value (unit: dB). Since the maximizing procedure for the  $S/N$  ratio minimizes the press formability, the best conditions can be obtained by maximizing ( $\eta$ ). The factors to be considered here, to establish their effects on the press formability, are the die corner radius ( $R$ ), the declination of the bead punch ( $a$ ), and the peak angle of the bead punch ( $b$ ).

Figure 3.5 presents the definition of these three factors, while their selected levels are listed in Table 3.2.

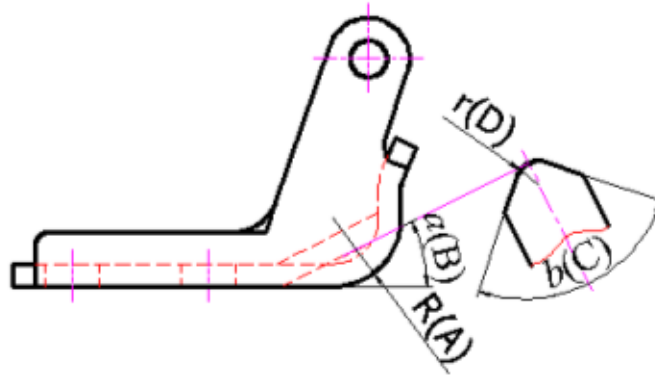


**Figure 3.5:** Definition of factors in concerned area

**Table 3.2:** Factors and their levels in FEM simulation

Factors	Level		
	1	2	3
A (R mm)	10	15	20
B ( $a^\circ$ )	14	22	30
C ( $b^\circ$ )	70	90	110

As the FE simulation using the three-level factors, an  $L_9$  array can indeed be used to design the experiment. Therefore, a minimum of nine tests were required to investigate the effect on the FE simulation. Table 3.3 shows the  $L_9$  orthogonal array chosen from Taguchi's standard-orthogonal-array Table. The number for each column is related to the level number for each factor. In this study, only the individual effects of each factor on the FE simulation were investigated, without considering the interactions between each factor.

**Table 3.3:** Taguchi's  $L_9$  orthogonal array for simulations

Case	A (R mm)	B ( $a^\circ$ )	C ( $b^\circ$ )
1	1(10)	1(14)	1(70)
2	1(10)	2(22)	2(90)
3	1(10)	3(30)	3(110)
4	2(15)	1(14)	2(90)
5	2(15)	2(22)	3(110)
6	2(15)	3(30)	1(70)
7	3(20)	1(14)	3(110)
8	3(20)	2(22)	1(70)
9	3(20)	3(30)	2(90)

### 3.4 Results and Discussion

When the softening property is used in constitutive models, the stress-strain relation defined in FE simulation must be adjusted with respect to element size, keeping the fracture energy constant. This adjustment of the stress strain relation with the element size is a way of incorporating fracture mechanics theory into finite element computation. If all elements were given the same softening stress-strain relation regardless of element size, the result would be mesh-dependent due to the inconsistent fracture energy treatment. On the contrary, when the material property can be defined as plasticity, the redistribution of stresses can occur as a result of plastic flow. Failure is define as occurring when the entire material volume reaches simultaneous yielding. In such a case, the constitutive models can be made independent of the element size. In our research, after several times reduced the mesh size to carry out the Table and reliable FE simulation results, we used the average element size of the blank element was about 1mm in width, 1mm in length, and 1mm in height. This mesh size is small enough to analyze the plastic deformation and failure of door hinge. The FE simulation results for a cracked test sample with the von Mises stress ( $\bar{\sigma}$ ), equivalent plastic strain ( $\bar{\epsilon}$ ), and the maximum ductile fracture value  $I$  (SDV9) calculated from Equation (3.3) via VUMAT user material based on isotropic hardening, kinematic hardening, and a combined isotropic/kinematic hardening law are presented in Figures 3.6(a), 3.6(b), and 3.6(c), respectively.

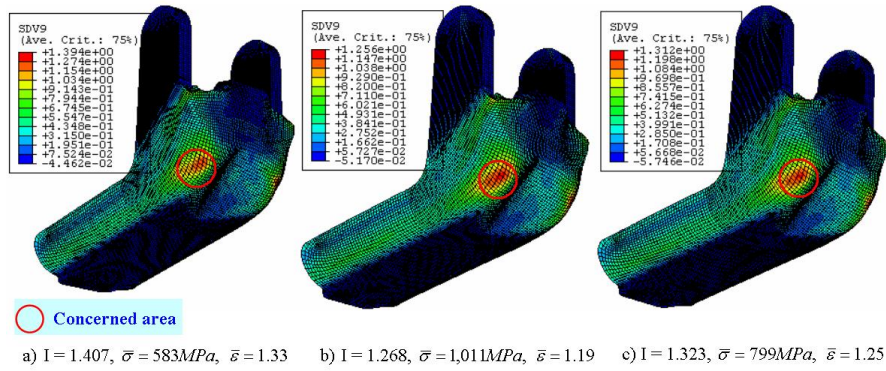


**Figure 3.6:** Deformed shapes of product failure in finite element simulation based on (a) isotropic hardening, (b) kinematic hardening, and (c) combined isotropic/kinematic hardening law.

The results show that the maximum ductile fracture values  $I$  were not so different, yet the maximum von Mises stresses ( $\bar{\sigma}$ ) in the concerned area for all the three hardening models were distinctly different. From the combined isotropic/kinematic hardening law, the von Mises stress in the concerned area was closest to the equivalent stress of tensile failure. So, the combined isotropic/kinematic hardening law will give better result when compared to other two hardening models. Figure 3.7 shows the evolutionary stress state at the element having maximum value of ductile fracture value  $I$  in the concerned area with the combined isotropic/kinematic hardening model for the case of  $R(A)=10\text{mm}$ ,  $a(B)=30^\circ$ ,  $b(C)=90^\circ$ , and  $r(D)=5\text{mm}$ .

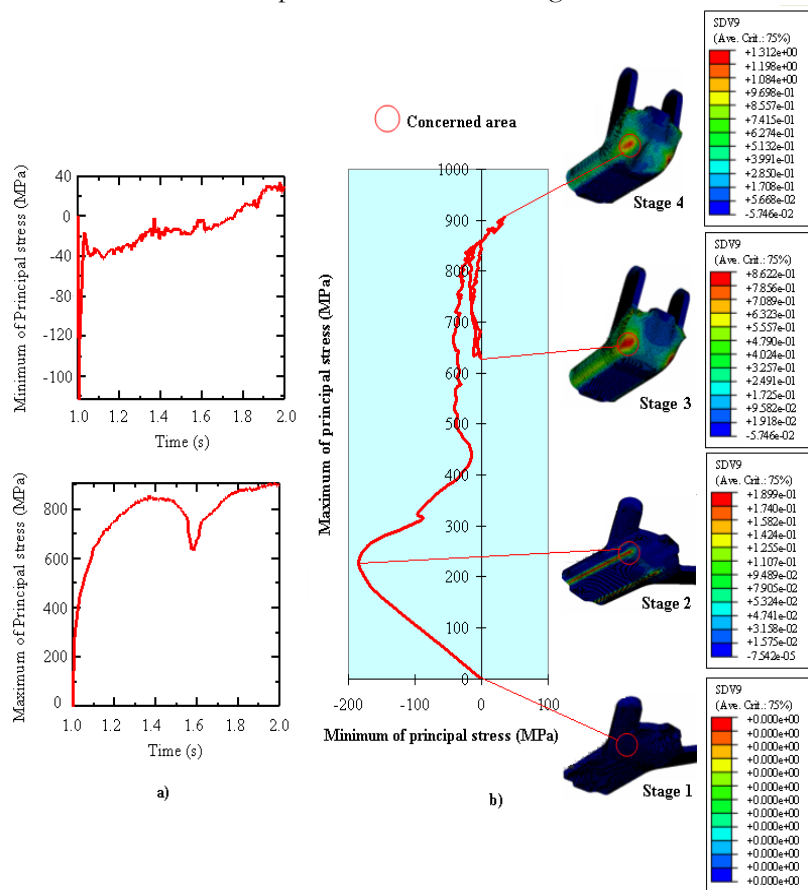


**Figure 3.7:** Evolutional stress state in concerned area

The evolutions of the maximum and minimum principal stress state at the element having maximum value of ductile fracture value I in the concerned area versus time are presented in Figure 3.7(a). Meanwhile, Figure 3.7(b) shows the stress path in the concerned area, which was complicated and also reversed between forming stage 2 and 3. Therefore, this complicated, reversed and nonlinear stress path in the concerned area supports the use of a combined isotropic/kinematic hardening law to predict the fracture of a door hinge.

In order to determine the scalar parameter  $\beta$ , the cyclic tensile curves, obtained by FE simulation via VUMAT user material through changing the values of  $\beta$ , was compared with experiment data and chosen the best fit as shown in Figure 3.8. The scalar parameter  $\beta$  for isotropic/kinematic hardening was estimated as 0.5.

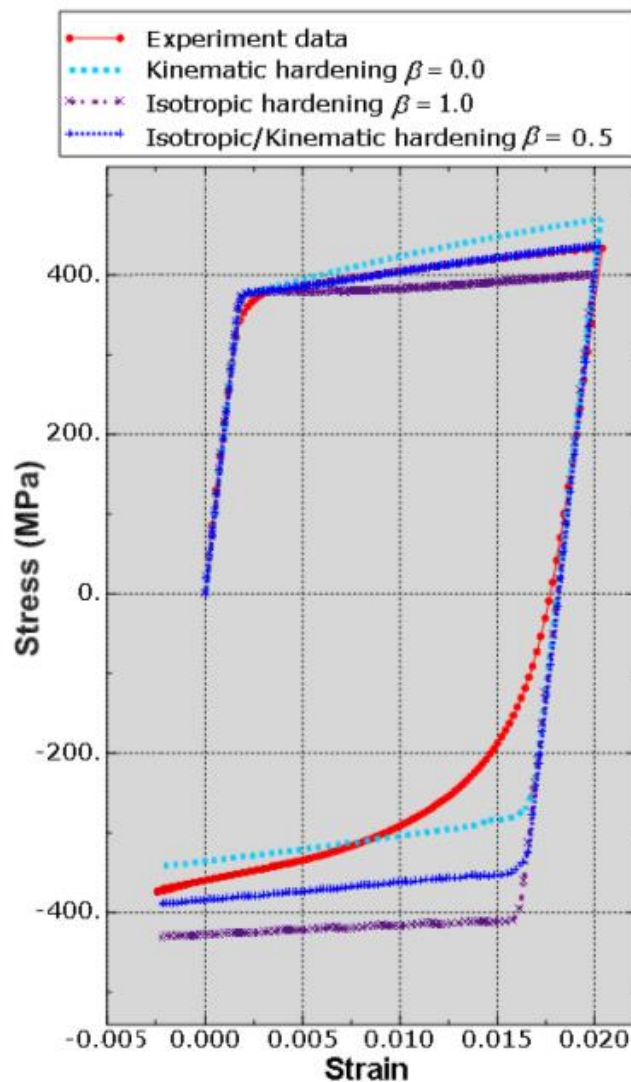


**Figure 3.8:** Estimation of scalar parameter ( $\beta$ )

Table 3.4 shows the results of the integral values  $I$  in numerical simulations based on a combined isotropic/kinematic hardening law for each case chosen from Taguchi's standard-orthogonal-array Table. The maximum value of the integral values  $I$ , i.e. the potential initial fracture site, appeared at the corner of the product for all cases. As mentioned before, the condition of failure was satisfied when and where the ductile fracture values  $I$  approached 1.0. For case no.2 and no.3, the ductile fracture values  $I$  were larger than 1.0, and failure appeared. The trends of the failure site predicted in this study were in good agreement with those in the actual product.

**Table 3.4:**  $L_9$  orthogonal array and calculated observed values

Case	Column number and factor assignment			Ductile fracture value (I)	
	A (R)	B (a)	C (b)	I	$\eta_i^a$ (dB)
1	1(10)	1(14)	1(70)	0.837	1.545
2	1(10)	2(22)	2(90)	1.007	-0.061
3	1(10)	3(30)	3(110)	1.343	-2.561
4	2(15)	1(14)	2(90)	0.815	1.777
5	2(15)	2(22)	3(110)	0.828	1.639
6	2(15)	3(30)	1(70)	0.843	1.483
7	3(20)	1(14)	3(110)	0.732	2.710
8	3(20)	2(22)	1(70)	0.743	2.580
9	3(20)	3(30)	2(90)	0.755	2.441

According to the Taguchi's method, an analysis of the mean (ANOM) and analysis of variance (ANOVA) were used to represent the relationship between the geometry factors for the concerned area and the observed values for the integral values  $I$ . In this experiment, the observed values were found to be related to the three parameters (Table 3.4). The optimization of the observed values was then determined through a comparison with the Taguchi signal-to-noise ( $S/N$ ) ratio. The ANOVA values calculated for the three factors and their corresponding three levels (tabulated in Table 3.2) were obtained using an  $L_9$  orthogonal array. The use of orthogonal array reduced the full factorial design down to 9 experiments from 81 experiments, thereby decreasing the cost, time, and effort. The increase in the factor effect was measured using the  $S/N$  ratio of the factors. Moreover, the analysis of the mean (ANOM) and analysis of variance (ANOVA) for the quality characteristics provided a better understanding of the individual effect of each factor. The ANOVA for the different factors - including the level average, total variation, sum of the squares, sum of the mean squares, and contribution - enabled various relative quality effects to be determined.

Tables 3.5 show a summary of the calculated results. The formulation used to calculate the sum of the squares was as follows:

$$3(m_{j1} - m)^2 + 3(m_{j2} - m)^2 + 3(m_{j3} - m)^2 \quad (3.5)$$

Where  $m$  is the overall mean of the  $\eta$ , value for the four experiments, defined as  $m = \frac{1}{9} \sum_{i=1}^9 \eta_i = 1.284$ , and  $m_{ji}$  is the average of  $\eta$  related to level  $i$  ( $i=1, 2, 3$ ) of factor  $j$  given by  $m_{ji} = \frac{1}{3} \sum_{i=1}^3 (\eta_j)_i$ .

The results of the ANOM and ANOVA for the ductile fracture values  $I$  (Table 3.5) revealed that the die corner radius (R), which reached 68.64%, made the major contribution to the overall performance. Meanwhile, the contribution percentages for the declination of the bead punch ( $a$ ) and peak angle of the bead punch ( $b$ ) were lower at 18.75% and 12.61%, respectively. The contribution percentage of the peak angle of bead punch ( $b$ ) was the smallest at 12.61%. Thus, it was concluded that the die corner radius (R) factor had the most significant effect on the ductile fracture value  $I$  in the concerned area.

**Table 3.5: ANOM and ANOVA Table of effect on ductile fracture value ( $I$ )**

Factor	Average $\eta$ by Level			Sum of Squares	D.O.F	Sum of mean squares	Contribution
	1	2	3				
A(R)	-0.359	1.633	2.577*	13.479	2	6.7395	0.6864
B( $a$ )	2.011*	1.386	0.454	3.683	2	1.8415	0.1875
C( $b$ )	1.869*	1.385	0.596	2.477	2	1.2385	0.1261
Total				19.639	6	9.8195	
* Indicates optimum level							

The  $\eta$  (dB) of the levels for each factor were individually calculated, as shown in Table 3.4. In the Taguchi method, the higher the  $\eta$  value, the better the overall performance, meaning that the factor levels with the highest  $\eta$  value should always be selected. Accordingly, the average for each experimental level was calculated using the highest  $\eta$  value for each factor to produce the response Table (Table 3.5). As shown in the response Table and response graph, the improved conditions to maintain the ductile fracture value  $I$  successfully in the forming test were  $A_3B_1C_1$ , which means  $R = 20$  mm,  $a = 14^\circ$ ,  $b = 70^\circ$ , and  $r = 5$  mm. The S/N ratio for these improved conditions is denoted by  $\eta_{opt}$  and predicted as Equation (3.6):

$$\eta_{opt} = m + (m_{A3} - m) + (m_{B1} - m) = 3.304(dB) \quad (3.6)$$

Figure 3.9 depicts the FE simulation results of the improved conditions ( $A_3B_1C_1$ ) for the press formability. Here, the equivalent stress, equivalent strain is decreased, and the integral value  $I$  has the minimum value. Figure 3.10 shows the experiment results for case No.8, where no crack appeared in the corner of the concerned area.

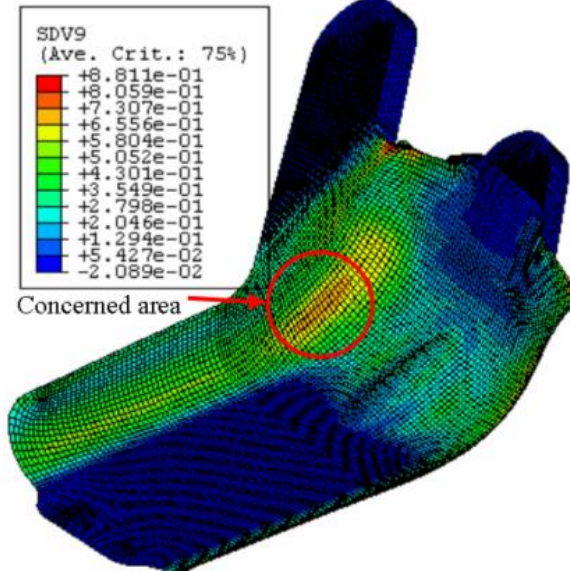


**Figure 3.9:** Deformed shape in finite element simulation of optimum case, where integral value  $I$  was 0.725 in concerned area



**Figure 3.10:** Case No. 8:  $R=20\text{mm}$ ,  $a=20^\circ$ ,  $b=90^\circ$ ,  $r=5\text{mm}$ ,  $I=0.748$ . No crack occurred in concerned area

From the above discussion, it was concluded that the use of Taguchi's experimental array for the FE simulations allowed successful improvement of the geometric shape of the die and bead punch in the concerned area to improve the press formability. As a result, the geometric shape of the die and bead punch in the area of concern was improved using a die corner radius (R) of 20 mm, declination of the bead punch ( $a$ ) of  $14^\circ$ , and peak angle of the bead punch ( $b$ ) of  $70^\circ$ .

### 3.5 Conclusion

To predict a fracture and improve the press formability of a door hinge, the geometric shape of the die and bead punch in the concerned area was improved using finite element simulations and then investigated by experiments. Commercial software (ABAQUS version 6.5, explicit formulation) with a user-defined subroutine (VUMAT) based on a combined isotropic/kinematic hardening model was used for the simulation according to the orthogonal array of Taguchi's method. As a result, the die corner radius (R) was identified as the important factor for improving the press formability of the door hinge. Improved geometric shapes for the die and bead punch in the concerned area, consisting of a die corner radius (R) of 20 mm, declination of the bead punch ( $a$ ) of  $14^\circ$ , and peak angle of the bead punch ( $b$ ) of  $70^\circ$ , were also predicted to produce a better reliability compared to the original test sample.